INTERNATIONAL JOURNAL
OF
CONSERVATION SCIENCE

ISSN: 2067-533X Volume 14, Issue 2, April-June 2023: 537-550 www.ijcs.ro

DOI: 10.36868/IJCS.2023.02.11

# INVESTIGATION ON THE SURFICIAL STAIN ABOVE THE OUTDOORS SANDSTONE SCULPTURE IN CHONGQING CHINA THREE GORGES MUSEUM

Xiong Wei ZHAO[1], Cun Chong SUN[1], Pu CHENG[2], Pu Jun JIN[2*]

[1] Chongqing China Three Gorges Museum, Chongqing 410010, China
[2] School of Materials Science and Engineering, Shaanxi Normal University, Xi'an 710119, China

***Abstract***

*A famous winged sandstone sculpture named Bixie of the Wei and Jin Dynasties (220 ~ 420 AD) is placed on the right side of the Chongqing Three Gorges Museum, accompanied by serious weathering on its surface. To explore the structural and compositional properties of the weathered, exfoliated, repaired cement, and yellow crust samples, scanning electron microscopy (SEM), X-ray diffraction (XRD), X-ray fluorescence spectrometer (XRF), Fourier transform infrared spectroscopy (FTIR), thermal analysis (TGA/DTG), and X-ray photoelectron spectrum (XPS) were applied to determine the efflorescence that occurred on the surface of sandstone sculpture and repair cement. The results show that a high concentration of gypsum was detected in the weathering sample, which indicated that the deterioration of the stone body of Bixie was caused by the combined action of internal salt crystallisation and external air pollution. Both $SO_2$ in the atmosphere and SO2-4 in acid rain react with substances containing calcium in sandstone to form anhydrite that causes expansion in volume, resulting in loosening and crisp powder on the surface of sandstone. The formation of the Fe-rich concretions and stagnant $Fe^{2+}$-rich water on the surface, reacting with sulphur oxides in the atmosphere, will cause the stone carving surface to turn yellow. Cement is prone to corrosion due to carbonization and corrosion of gypsum, so it is necessary to replace the cement in the subsequent repair. This study reveals the properties of the surficial stain above the sandstone sculpture in the Chongqing China Three Gorges Museum, providing important information for their protection and restoration.*

***Keywords****: Outdoor cultural relic; Stone cultural relics; Sandstone; Weathering; $CaSO_4 \cdot 2H_2O$; Air pollution*

## Introduction

A winged sandstone sculpture, named Bixie as a mythical animal and considered a protection against evil spirits, is 183cm high, 70cm wide, and 289cm long and is placed on a rectangular stone platform in the open air without any shelter. After a long period of pollution by the atmospheric environment, the sandstone body of the sculpture and the prior cement used to repair cracks have suffered from efflorescence.

In an open environment, the stone carvings will be eroded by many natural factors such as acid rain [1], soluble salts [2, 3], harmful gases [4], temperature and humidity changes [5, 6], dust [7], microorganisms [8], ultraviolet rays [9-11] in the atmospheric environment [12, 13], etc.

As a warm district in southern China, Chongqing city has a subtropical monsoon humid climate, with an annual average temperature of 16–18℃ and an annual average relative

* corresponding author: jinpj@snnu.edu.cn

humidity of 70–80%. Acid rain, acid fog, and water seepage are the two major weathering agents that cause the destruction of sandstone carvings in this district [14, 15]. The atmospheric pollutants, including sulphur and nitrogen oxides, will cause acid deposition as wet deposition in the form of acid rain, acid snow, or acid fog and as dry deposition [16]. Therefore, soluble salts have accumulated in sandstone over the years, either because of reactions of the stone with atmospheric pollutants or capillarity [17]. Exposure tests using fresh stone have indicated that stone sulfation is most rapid immediately subsequent to exposure [16, 18], and rain washing slows the accretion of organic matter and dissolution of soluble minerals but markedly increases the rate of surface gypsum accumulation [19].

This paper focuses on the efflorescence that occurred on the surface of sandstone sculpture and repair cement in order to reveal the weathering characteristics of the stone body of Bixie, its weathering mechanism by atmospheric pollutants, and its further conservation.

## Materials and methods

### *Materials*

Figure 1 shows the picture of the sandstone Bixie (Fig. 1a) with the efflorescent leg (Fig. 1b), the repair concrete (Fig. 1c), and the mouth with yellow staining (Fig. 1d). The efflorescence of sand sculpture is observed on the inside of its right hind calf, where rain can't wash and will accumulate the soluble salts by rainwater infiltration and diffusion. The efflorescence sample from its right hind calf, the exfoliation sample from its platform, the repair concrete from its neck, and the yellow crust from its mouth were collected to evaluate the weathering properties of this sand sculpture in the open storage environment, as listed in Table 1.


**Fig. 1.** The picture of Bixie (a), the efflorescent sample from the right hind calf (b), the repair concrete (c) and the mouth with a yellow crust (d)

**Table 1.** The description of samples

| Number | Name | Statue | Place |
|---|---|---|---|
| 1 | Efflorescence sample | Powdery particle | From the calf |
| 2 | Exfoliation sample | Sheet fragments | From the platform |
| 3 | Repair concrete | Bulk fragments | From the repair concrete in the neck |
| 4 | Yellow crust | Powdery particle | From the mouth |

***Methods***

The sample compositional analysis was measured using an energy dispersive X-ray fluorescence spectrometer (Shimadzu's EDX-7000) equipped with an Rn target and a silicon drift detector ranging from elements Na to U.

The sample phases were analysed using XRD via a Rigaku Smart Lab X-ray diffractometer equipped with Cu Kα radiation and recorded in the 2θ range from 5° to 80° with a tube voltage of approximately 40 kV and a current of approximately 30mA.

Fourier-transform infrared spectra (FT-IR) were obtained using a Bruker Tensor 27 spectrometer with the samples dispersed in KBr in the range of 400～4000$cm^{-1}$.

A Quanta 200 scanning electron microscope equipped with an X-ray energy dispersive spectrometer (EDS) was applied to detect the elemental mapping in samples under a high vacuum mode (< $5.0\times10^{-3}$Pa).

The samples were investigated via a simultaneous TGA/DSC equipment (SDT-Q600) with a sample quantity of about 5～10mg ranging from 30 to 1450°C at a heating rate of 10°C/min under $N_2$ atmosphere.

X-ray photoelectron spectroscopy (XPS) was performed to study the chemical state of the main elements in the weathered materials using a Kratos Axis Ultra X-ray photoelectron spectrometer with an Al Kα (1486.7eV) excitation source.

## Results and discussion

***XRF analysis***

The XRF results, shown in Table 2, reveal a higher concentration of elements S and Ca in efflorescence sample No. 1 than that in exfoliation sample No. 2, corresponding to the corrosive sulphate ($CaSO_4$).

**Table 2.** Sample elemental composition analysed by XRF（wt. %）

| Sample | Si | Ca | Al | S | Fe | Mg | Na |
|---|---|---|---|---|---|---|---|
| No.1 | 39.15 | 23.84 | 13.34 | 9.09 | 7.95 | 3.18 | 1.51 |
| No.2 | 51.88 | 18.02 | 13.30 | 4.41 | 6.45 | 2.74 | 1.80 |
| No.3 | 88.73 | / | 5.64 | 0.85 | 1.66 | 0.47 | / |
| No.4 | 58.06 | 4.85 | 15.05 | 0.87 | 11.15 | 3.01 | 2.05 |
| **Sample** | **Ti** | **Mn** | **P** | **Zr** | **Cr** | **K** | |
| No.1 | 1.24 | 0.31 | 0.28 | 0.11 | / | / | |
| No.2 | 0.70 | 0.49 | / | / | 0.21 | / | |
| No.3 | 0.59 | / | 0.33 | / | / | 1.72 | |
| No.4 | 1.02 | 2.50 | 1.26 | / | 0.18 | / | |

It is reported that a sandstone lion prior to being covered by a layer of organic protective coating showed a higher concentration of S, about 14.25%, on the back of this weathering protective coating, which also would accumulate the sulphate [20, 21]. Therefore, the accumulation of gypsum is the key mechanism for the sulphur corrosion phenomenon that will cause the micronization and exfoliation of the stone surface in this case.

Sample No. 3 is the repair concrete with a high concentration of Si, about 88.73%, which reflects a quantity of sand used as fillers in repair cement and a release of cement composition. A major factor in concrete decay is carbonation by carbon dioxide ($CO_2$), which destroys its

alkaline substance in the atmosphere and affects concrete durability [21]. In this case, the carbonation process would release the main composition of concrete, accompanied by the leaching action of rainwater, such as elements Ca and Al.

The yellow crust is observed on the surface of the sand sculpture, and the high concentration of element Fe, about 11.15%, is detected in Sample No. 4, corresponding to the iron salt deposit.

***XRD analysis***

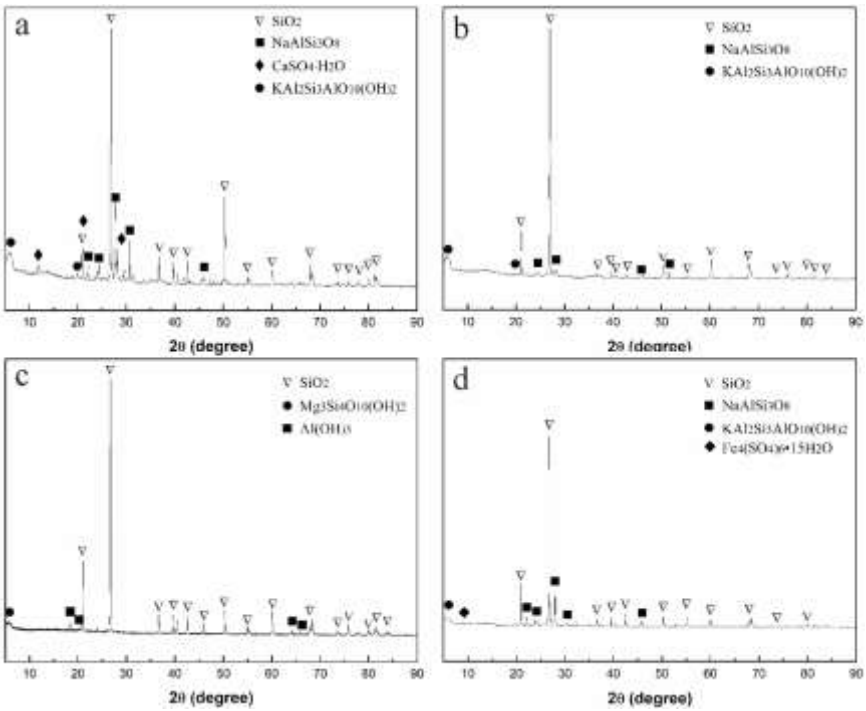


**Fig. 2.** The XRD patterns of Bixie, the efflorescent sample from the right hind calf (a), exfoliation sample from the platform (b), the repair concrete (c), and the mouth with yellow crust (d)

As shown in Figure 2a, the XRD pattern of the efflorescent sample for the right hid calf shows the existence of quartz ($SiO_2$), alibite [$Na(AlSi_3O_8)$], muscovite [$KAl_2Si_3AlO_{10}(OH)_2$], and gypsum ($CaSO_4$•$2H_2O$). Gypsum is an important salt cause of chemical weathering for sandstones [21], which comes from sulphide in the atmosphere, indicating that the main salt on the surface of sandstone Bixie is sulphate.

Peaks appearing in Figures 2b and d are similar to those in Figure 2a; they can be indexed to quartz ($SiO_2$), alibite [$Na(AlSi_3O_8)$], and muscovite [$KAl_2Si_3AlO_{10}(OH)_2$], which is the material composition of a sandstone body. The difference is that Figure 2c shows the existence of $Al(OH)_3$, probably due to the element Al released in the carbonation process of the repair concrete.

As Balsamo reported, when $O_2$ diffuses into stagnant $Fe^{2+}$-rich water, it causes the formation of Fe-rich concretions [22], and stagnant $Fe^{2+}$-rich water on the surface reacts with sulphur oxides in the atmosphere. So $Fe_4(SO_4)_6{\cdot}15H_2O$ is detected, and $Fe^{3+}$ is a colour component in the yellow crust, as shown in figure 2d.

### *FTIR analysis*

FTIR spectroscopy was employed to obtain the qualitative characteristics of weathering shown in Figure 3, and the assignment of the absorption bands is shown in Table 3.

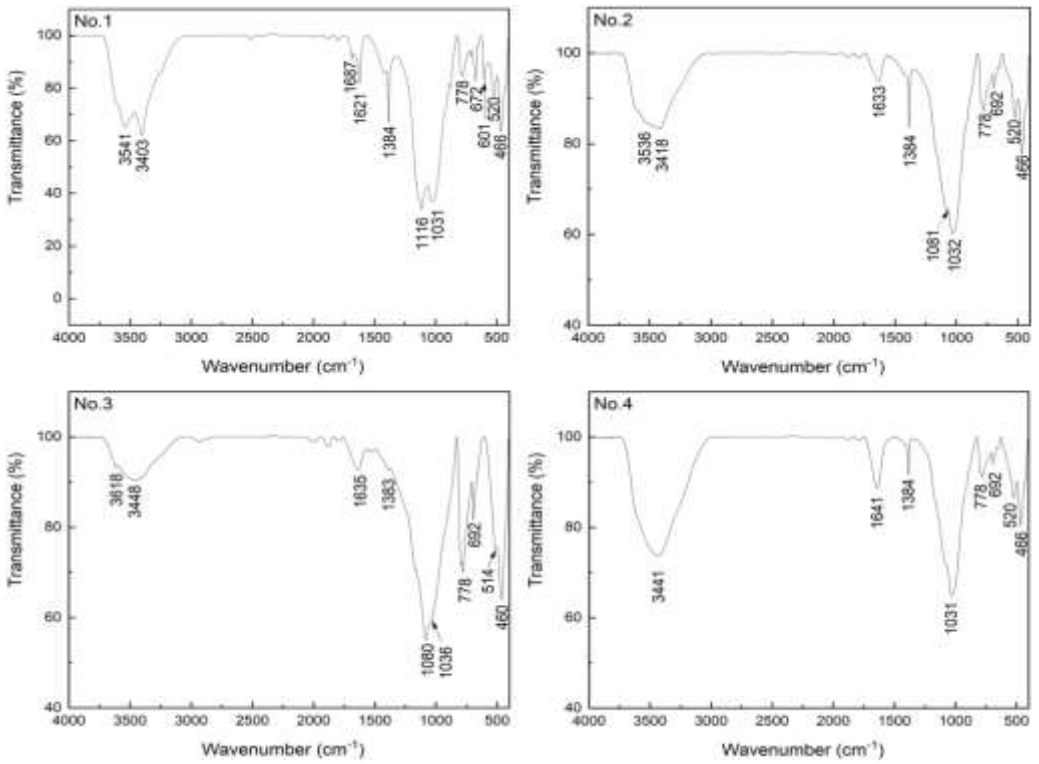


**Fig. 3.** FTIR spectra, the efflorescent sample (No. 1), the exfoliation sample (No. 2), and the repair concrete (No. 3) and the yellow crust (No. 4).

For sample No. 1, the presence of IR absorption peaks at 466, 601, 672, 1116, 1621, 1687, 3403, and 3541cm$^{-1}$ are corresponding to gypsum ($CaSO_4$•$2H_2O$). It was shown in sample No. 1–4 that the band at 1031cm$^{-1}$ arises from stretching vibrations of sialic acid salts. The 1384cm$^{-1}$ sharp band is the fundamental $\nu_3$ characteristic of alkali and alkaline earth nitrates [23]. For sample No. 3, the peak at 3618cm$^{-1}$ is belongs to the OH-stretching vibrations from $Al(OH)_3$ groups [24]. The peaks at 778 and 1081cm$^{-1}$ detected in samples No. 2 and No. 3 are ascribed to quartz ($SiO_2$). An intense absorption band located at 1635cm$^{-1}$ due to the bending H-O-H of water molecules attributed to the formation of the hydrated silicate. A wide band at around 3436cm$^{-1}$ generated by O–H bond stretching vibration associated with the water molecules from the hydrated silicate [25].

**Table 3.** Compounds detected by FTIR analysis

| Compound | Fundamentals | | | | O-H | H-O-H |
|---|---|---|---|---|---|---|
| | $\nu_1$ | $\nu_2$ | $\nu_3$ | $\nu_4$ | $\nu$ | $\delta$ |
| Gypsum | | 466 | 1116 | 672, 601 | 3403, 3541 | 1621, 1687 |
| Quartz | 778 | 520 | 1081 | | | |
| Feldspars | | | 1031 | | | |
| Nitrates | | | 1384 | | | |
| $Al(OH)_3$ | | | | | 3618 | |

***Thermal analysis***

The TG analysis results of the samples are shown in Figure 4. The variations that occurred at temperatures below l00°C were due to surface-adsorbed $H_2O$ [26]. Additional gypsum decomposition occurred between 100 and 130°C, with a weight loss of approximately 0.04% in sample No. 1, reaching the maximum decomposition rate at 118°C [27]. The weight loss between 280 and 370°C is related to the deacidification and dehydrogenation of organic components [28]. The small endothermic peak at 410°C reflects the decomposition of silicate [29]. In the region of each of the DTG curves, the weight loss is centred at the temperature interval of 450–600°C. Peaks at 548°C in the sample No. 2, 490°C in the sample No. 3, and 534°C in the sample No. 4 correspond to the dihydroxylation of aluminosilicate, such as Muscovite [$KAl_2Si_3AlO_{10}(OH)_2$]. However, addition peaks at 68°C in the sample No. 1, 703°C in the sample No. 3, and 701°C in the sample No. 4 were detected, which is likely to correspond to a more thermally stable and more ordered polymorph of aluminosilicate [30-32].

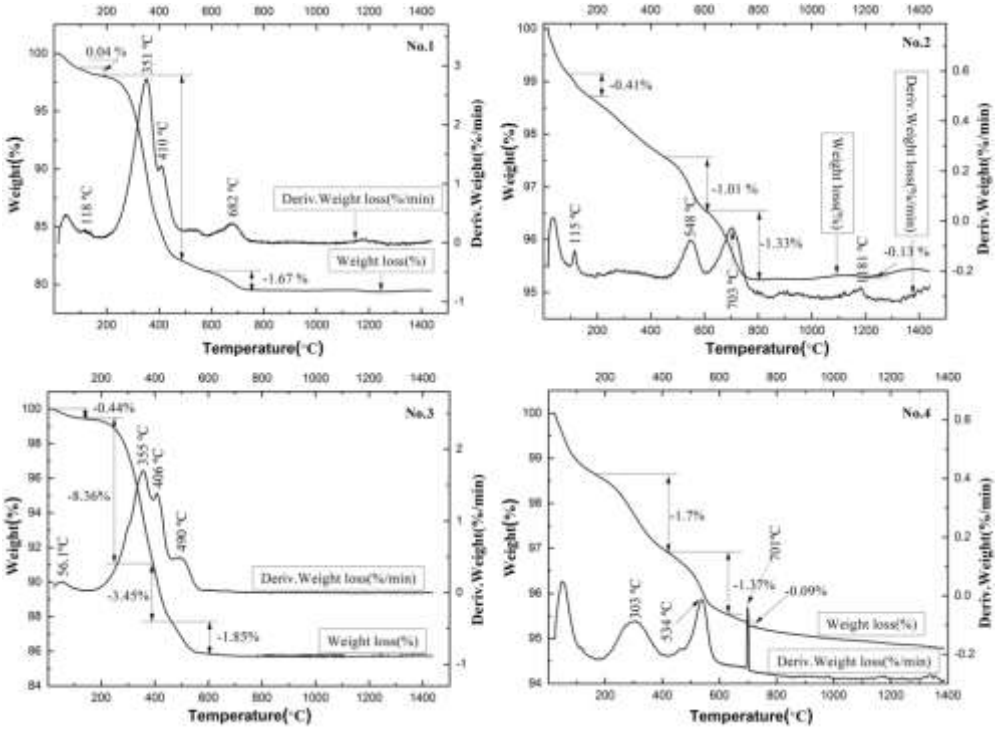


**Fig. 4.** TG plots of analyzed samples

In the range 450–750°C of the DTG curves, a dehydroxylation process is observed, hydroxyl groups in the mineral structure of the sandstone were lost as water, and structural water was also lost in the process.

***EDS mapping analysis SEM results***

The efflorescent sample is observed on the inside of its right hind calf, where rain can't wash and will accumulate the soluble salts by rainwater infiltration and diffusion. Figure 5 shows the elemental distribution mapping, from which the surface morphology and distribution information of each component can be obtained.

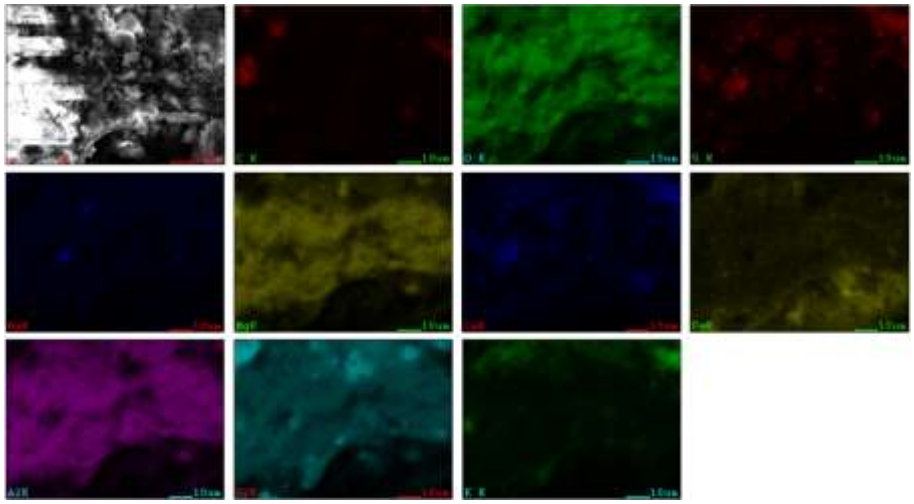

**Fig. 5.** SEM-EDS maps of the efflorescent sample from the right hind calf (No. 1)

It showed that the distribution pattern of Ca was consistent with the distribution pattern of S, corresponding to the existence of $CaSO_4$. The distribution pattern of Si showed that the areas with high Si content are dispersed, which indicates that the salt damage has completely destroyed the body structure of cultural relics.

The exfoliated sample was collected from the platform of Bixie. The SEM-EDS elemental distribution maps of sample No. 2 are shown in Figure 6.

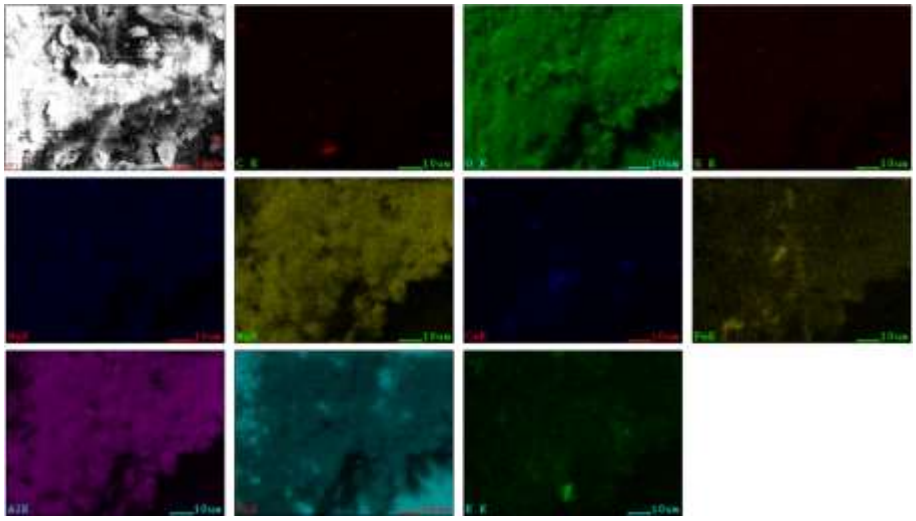

**Fig. 6.** SEM-EDS maps of the exfoliated sample from the platform (No. 2)

It showed that the distribution patterns of C and S are relatively uniform, which reflected that the salt has not formed a bigger aggregate. And the area with a high content of Si became tiny. The distribution of high-content Al and Si elements is characterised by a regional surface, and there are many fine holes among the particles, showing loose microstructure.

The repair concrete sample was collected from the neck of the Bixie. The SEM-EDS elemental distribution maps of sample No. 3 are shown in Figure 7.

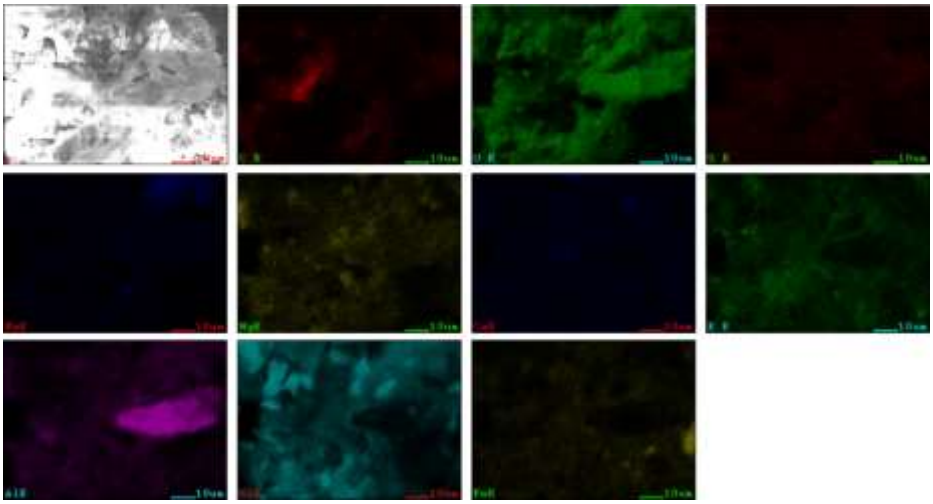

**Fig. 7.** SEM-EDS maps of the repaired concrete (No. 3)

It indicated that the sample had a porous stacking structure. The distribution of Al in large areas was related to the aluminate in cement. The cement is mainly composed of $CaO•SiO_2•Al_2O_3$ and $Fe_2O_3$. The $CaO•SiO_2•Al_2O_3$ and $Fe_2O_3$ in clinker do not exist as separate oxides but as aggregates of various minerals formed by two or more oxides through high-temperature chemical reactions. They are mainly tricalcium silicate ($3CaO•SiO_2$), dicalcium silicate ($2CaO•SiO_2$), Tricalcium aluminate ($3CaO•Al_2O_3$), and tetracalcium ferroaluminate ($4CaO•Al_2O_3•Fe_2O_3$). Usually, the content of tricalcium silicate and dicalcium silicate in clinker is about 75%, and the theoretical content of tricalcium aluminate and tetracalcium ferroaluminate accounts for about 22%.

The yellow crust sample was collected from the mouth of the Bixie. The SEM-EDS elemental distribution maps of sample No. 4 are shown in Figure 8.

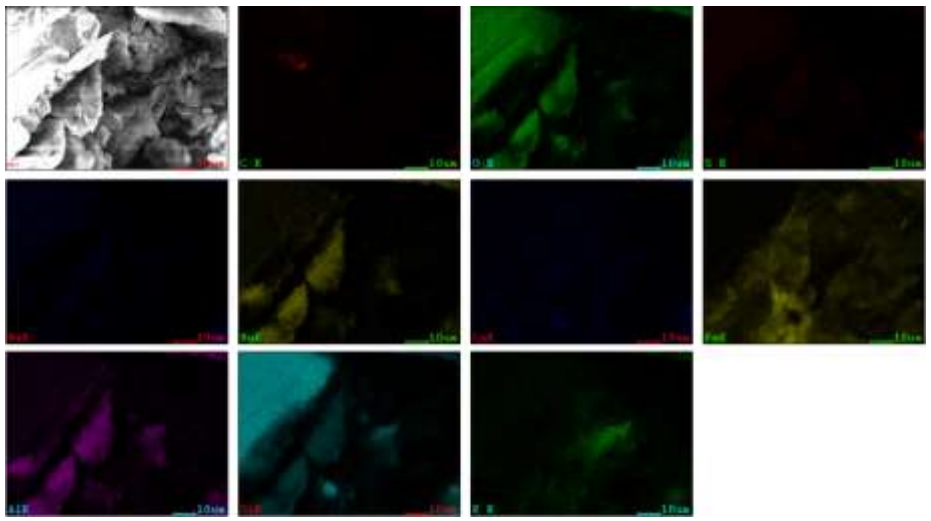

**Fig. 8.** SEM-EDS maps of the yellow crust from the mouth (No. 4)

It indicated that the sample is mainly composed of Si, O, and Al with a multi-layer flake crystal accumulation structure. This morphology is significantly different from the granular sandstone body, which is likely due to the crusty material formed by water-soluble silicate. The distribution patterns of O, Si, Mg, and Al are similar, while the distribution pattern of Fe, which is distributed outside the areas of O, Si, Mg, and Al, is obviously different. Fe is an important element for the colour of yellow crusts.

***X-ray photoelectron spectroscopy (XPS)***

X-ray photoelectron spectroscopy (XPS) was used to characterise the chemical state of the element on the surface of samples No. 1, No. 2, No. 3, and No. 4. C, O, Ca, Al, Si, Mg, S, Na, and K were detected, as shown in Figure 9. The spectra were corrected by using the C 1s peak at 284.8eV.

Figure 9 shows the XPS survey scans and the atomic concentration was listed in Table 4. These samples were very similar in atomic composition, the Si 2p peak at energy binding of 102.85eV, assigned to $SiO_2$ and the O 1s spectrum has a main component at approximately 532.02eV, which includes the contribution of $SO_3^{2-}$, $SO_4^{2-}$ and $OH^-$ ions. For the No.1, a weak peak at 407.37eV is related to nitrates. The binding energy for the S 2p peak at 169.3eV belongs to $SO_4^{2-}$ and the Ca 2p3/2 perk was observed at 347.8eV assigning to gypsum ($CaSO_4 \cdot 2H_2O$) [33, 34].

The components of the exfoliated sample No. 2 are similar to those shown in No. 1, but the atomic concentration of S and Ca is lower than that of No. 1, while the atomic content of N and Cl is higher. A weak peak at approximately 197.77eV is related to chloride. The N 1s peak at approximately 400eV corresponds to organic components containing N due to air pollution. For the repair concrete sample, the peak at 74.25eV is attributed to Al 2p3/2, and O 1s was also detected at 532.17eV, indicating the existence of $Al(OH)_3$.

Figure 9 (g, I) shows the XPS spectra of Fe to explore the colour components of the yellow crust. The peak at 169.01eV is due to S 2p3/2 in $Fe_4(SO_4)_6 \cdot 15H_2O$ and Fe 2p3/2 can also be observed at approximately 713eV [35].

The results show the efflorescence sample No. 1 from the calf had a high content of S and Ca, which exist as gypsum, and the concentration areas of Si and Al are relatively dispersed. Compared to sample No. 1, the concentration areas of Si and Al in sample No. 2 became smaller and dispersed, which indicated the surface of the sandstone had become loose, which then caused the increase in cracks. It indicated the destructive effect of air pollution on sandstone.

The harmful components in the atmosphere are mainly $CO_2$, $SO_2$, and $NO_2$. Ca exists as calcareous cementitious material in sandstone; in the case of $CO_2$ and water, it will form $CaCO_3$, and then further dissolve into soluble $Ca(HCO_3)_2$（$CaCO_3 + CO_2 + H_2O \rightarrow Ca(HCO_3)_2$. This process will lead to the loss of Ca and directly cause the deterioration of sandstone. The $SO_2$ in the atmosphere and $SO_4^{2-}$ in acid rain can contact the surface of sandstone and even penetrate into the interior of sandstone and react with substances containing calcium to form $CaSO_4$. Anhydrite ($CaSO_4$) will form gypsum ($CaSO_4 \cdot 2H_2O$) after hydration, which will expand in volume during hydration, resulting in loosening and crisp powder on the surface of sandstone.

Due to the influence of sandstone's own materials such as porosity and permeability, the formation of the Fe-rich concretions and stagnant $Fe^{2+}$-rich water on the surface was easy to react with sulphur oxides in the atmosphere, and $Fe_4(SO_4)_6 \cdot 15H_2O$ was also detected in XRD and XPS, which caused the stone carving surface to turn yellow.

The concrete was widely used as a repair material in the repair process of this sculpture. Sample No. 3 is the repair concrete from the repair concrete in the neck of the sculpture. The XRF results showed a high content of Si, about 88.73%. The XRD and IR results showed that it was silica, aluminosilicate, and aluminium hydroxide. Only XPS results showed Ca was found in the form of gypsum ($CaSO_4 \cdot 2H_2O$), and the content was 0.13%. It was caused by the carbonization of cement and the corrosion of gypsum.

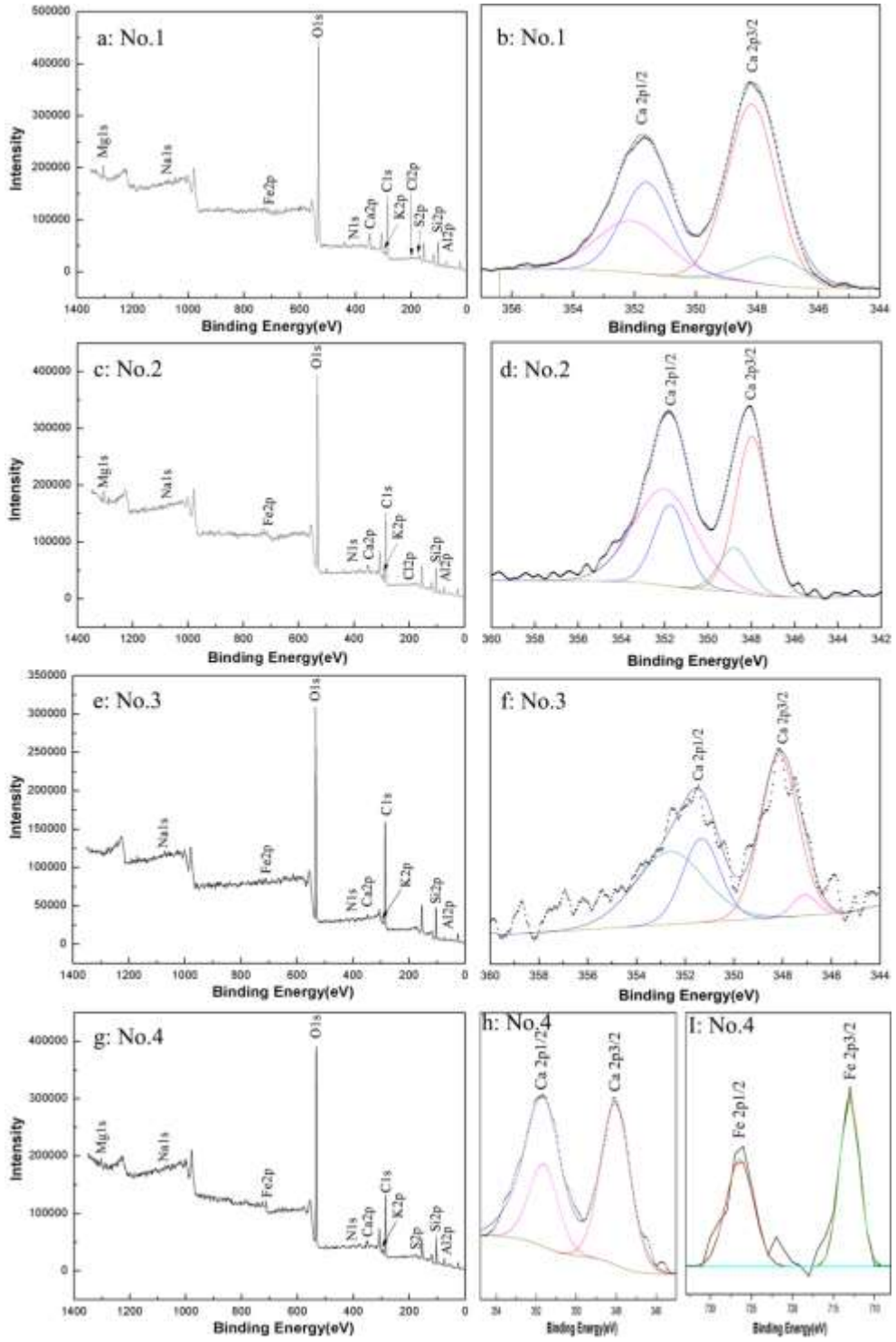


**Fig. 9.** XPS survey spectra of No. 1, No. 2, No. 3, and No. 4, and XPS spectra of Ca 2p and Fe 2p.

**Table 4.** The spectra listed with atoms, binding energy of peak and atomic concentration (at.%)

| Atoms | No. 1 | | No. 2 | | No. 3 | | No. 4 | |
|---|---|---|---|---|---|---|---|---|
| | Peak(eV) | at(%) | Peak(eV) | at(%) | Peak(eV) | at(%) | Peak(eV) | at(%) |
| O1s | 532.02 | 44.63 | 532.01 | 41.64 | 532.17 | 36.76 | 531.93 | 44.19 |
| C1s | 284.85 | 29.77 | 284.81 | 34.34 | 284.85 | 44.04 | 284.84 | 28.96 |
| Si2p | 102.85 | 13.39 | 102.83 | 13.5 | 102.98 | 14.36 | 102.79 | 14.34 |
| Mg1s | 1304.06 | 1.63 | 1303.89 | 1.76 | / | / | 1303.36 | 0.67 |
| Al2p | 74.21 | 5.97 | 74.12 | 5.46 | 74.25 | 2.77 | 74.53 | 6.75 |
| Ca2p | 348.02 | 2.54 | 347.62 | 0.18 | 347.18 | 0.12 | 346.92 | 0.17 |
| Na1s | 1070.82 | 0.27 | 1070.27 | 0.61 | 1070 | 0.52 | 1071.25 | 0.59 |
| K2p | 293.23 | 0.18 | 293.42 | 0.71 | / | / | 293.41 | 0.36 |
| N1s | 407.37 | 0.37 | 399.78 | 0.77 | 400.28 | 0.87 | 400.03 | 1.57 |
| Cl2p | 200.08 | 0.19 | 197.77 | 0.5 | / | / | / | / |
| S2p | 169.3 | 0.55 | / | / | / | / | 169.01 | 0.38 |
| Fe2p | 711.57 | 0.51 | 712.87 | 0.53 | 709.25 | 0.56 | 712.3 | 2.02 |

The main components of concrete are tricalcium silicate ($3CaO•SiO_2$), dicalcium silicate ($2CaO•SiO_2$), tricalcium aluminate ($3CaO•Al_2O_3$), and tetracalcium ferroaluminate ($4CaO•Al_2O_3•Fe_2O_3$). The process of concrete carbonization is as follows: the calcium hydroxide from concrete hydration with strong alkalinity and can react with $CO_2$ and water in the atmosphere to produce calcium carbonate, which is neutral. The corrosion of gypsum starts from the reaction of $SO_4^{2-}$ and calcium hydroxide: $Ca(OH)_2 + SO_4^{2-} \rightarrow CaSO_4$. The volume expansion and internal cracking caused by this process are the main factors causing cement damage [36].

## Conclusions

Combined with XRD, FTIR, TG, SEM-EDS, XPS, and other analytical methods, the weathered, exfoliated, repaired cement, and yellow crust samples from a winged sandstone sculpture in an outdoor setting were studied to determine composition, structure, and morphology.

Affected by air pollutants, not only the main components of sandstone, such as silica and aluminosilicate, but also traces of calcium sulphate and organic pollutants were detected in the weathered and exfoliated samples. It indicated that the black crust formed by weathering on the surface of sculpture was related to the carbonization of organic matter in the protective layer, and a high concentration of gypsum was accumulated under the crust. The volume of sculpture expanded in the hydration process of anhydrite to gypsum. These factors caused the surface looseness and crisp powder of the sculpture.

$Fe_4(SO_4)_6·15H_2O$ was the coloured substance of the yellow crust from the mouth, which caused the stone carving surface to turn yellow. Cement is easy to deteriorate due to carbonization and corrosion of gypsum in outdoor environments, so it is not suitable to be used as a cultural relic repair material and should be replaced in the follow-up repair.

## Funding

The study was supported by the Key Research and Development Programme of Shaanxi (Programme No. 2020SF-355), the Key Science & Technology Innovation Team of Shaanxi Province (2022TD-35 and 2023CXTD27), and the Fundamental Innovation Project in School of Materials Science and Engineering (SNNU).

## References


[1] E. Franzoni, E. Sassoni, *Correlation between microstructural characteristics and weight loss of natural stones exposed to simulated acid rain*, **Science of the Total Environment**, **412-413**, 2011, pp. 278-285. DOI: 10.1016/j.scitotenv.2011.09.080.

[2] C. Cardell, F. Delalieux, K. Roumpopoulos, A. Moropoulou, F. Auger, R. Van Grieken, *Salt-induced decay in calcareous stone monuments and buildings in a marine environment in SW France*, **Construction and Building Materials, 17**(3), 2003, pp. 165-179. DOI: 10.1016/s0950-0618(02)00104-6.

[3] B. Ratoi, V. Pelin, I. Sandu, M. Branzila, I.G. Sandu, *Hidden Message in Stone Masonry of Galata Monastery - Iasi City, Romania*, **International Journal of Conservation Science, 9**(1), 2018, pp. 151-164.

[4] F. Sitzia, C. Lisci, J. Mirão, *Building pathology and environment: Weathering and decay of stone construction materials subjected to a Csa mediterranean climate laboratory simulation*, **Construction and Building Materials, 300**(7), 2021, pp. 124311. DOI: 10.1016/j.conbuildmat.2021.124311.

[5] S. Siegesmund, K. Ullemeyer, T. Weiss, E.K. Tschegg, *Physical weathering of marbles caused by anisotropic thermal expansion*, **International Journal of Earth Sciences, 89**, 2000, pp. 170-182. DOI: 10.1007/s005310050324.

[6] M.M. Cazacu, V. Pelin, I. Radinschi, I. Sandu, V. Ciocan, I.G. Sandu, S. Gurlui, *Effects of Meteorological Factors on the Hydrophobization of Specific Calcareous Geomaterials from Repedea - Iasi Area, Under the Urban Ambiental Air Exposure*, **International Journal of Conservation Science, 11**(4), 2020, pp. 1019-1030.

[7] M. Mutlutürk, R. Altindag, G. Türk, *A decay function model for the integrity loss of rock when subjected to recurrent cycles of freezing–thawing and heating–cooling*, **International Journal of Rock Mechanics and Mining Sciences, 41**(2), 2004, pp. 237-244. DOI: 10.1016/s1365-1609(03)00095-9.

[8] K. Torfs, R. Van Grieken, *Chemical relations between atmospheric aerosols, deposition and stone decay layers on historic buildings at the mediterranean coast*, **Atmospheric Environment, 31**(15), 1997, pp. 2179-2192. DOI: 10.1016/s1352-2310(97)00038-1.

[9] V. Pelin, I. Sandu, S. Gurlui, M. Brinzila, V. Vasilache, I.G. Sandu, *Evaluation of the Artificial Aging Rate Through UV Radiation Exposure of Indigenous Carbonate Rocks, Treated with Water-solvated Nano-dispersions, with the Interest of Consolidation and the Formation of a Waterproof Character*, **Revista de Chimie, 67**(12), 2016, pp. 2568-2572.

[10] A. Cocean, V. Pelin, M.M. Cazacu, I. Cocean, I. Sandu, S. Gurlui, F. Iacomi, *Thermal effects induced by laser ablation in non-homogeneous limestone covered by an impurity layer*, **Applied Surface Science, 424,** 2017, pp. 324-329, Special Issue SI, Part 3. DOI: 10.1016/j.apsusc.2017.03.172.

[11] B. Laurenz, B. Nico, K. Tim De, C. Veerle, *The capabilities of bacteria and archaea to alter natural building stones – A review*, **International Biodeterioration & Biodegradation, 165**, 2021, pp. 105329. DOI: 10.1016/j.ibiod.2021.105329.

[12] V. Pelin, I. Sandu, S. Gurlui, M. Branzila, V. Vasilache, E. Bors, I.G. Sandu, *Preliminary investigation of various old geomaterials treated with hydrophobic pellicle*, **Color Research and Application, 41**(3), 2016, pp. 317-320, Special Issue SI, DOI: 10.1002/col.22043.

[13] B. Fsa, B. Cla, B. Jma, *Accelerate ageing on building stone materials by simulating daily, seasonal thermo-hygrometric conditions and solar radiation of Csa Mediterranean climate*, **Construction and Building Materials, 266**, 2021, pp. 121009. DOI:10.1016/j.conbuildmat.2020.121009.

[14] T. Navrátil, Z. Vařilová, J. Rohovec, *Mobilization of aluminum by the acid percolates within unsaturated zone of sandstones*, **Environmental Monitoring and Assessment,**

**185**(9), 2013, pp. 7115–7131. DOI: 10.1007/s10661-013-3088-4.
[15] D.Y. Wang, Z.X. Zhang, L.S. Fu, J.S. Yao, B.L. Xie, X.F. Yan, *Formation and distribution characteristics of acid rain in Dazu County and its damage to stone carvings*, **Hydrogeology and Engineering Geology, 3**, 1995, pp. 9-24. DOI：CNKI:SUN:SWDG.0.1995-03-003.
*[16]* G.*B. Rao*, *Effect of pollution by sulphur dioxide on marble and sandstone*, *Journal of* **Archaeological Chemistry, 1**(1), 1983, Article Number: 3. DOI: 10.1016/j.net.2021.06.011.
[17] R.J. Flatt, F. Caruso, A.M. Sanchez, G.W. Scherer, *Chemomechanics of salt damage in stone*, **Nat Commun, 5**, 2014, Article Number: 4823. DOI: 10.1038/ncomms5823.
[18] S.T. Brüggerhoff, P.W. Mirwald, *Examination of complex weathering V processes on different stone materials by 8eld exposure studies*, **Proceedings of the Seventh International Congress on Deterioration and Conservation of Stone,** (Editors: J.D.H Rodrigues**,** F.T. Jeremias), Lisbon, 1992, pp. 715–24.
[19] A.V. Turkington, E. Martin, H.A. Viles, B.J. Smith, *Surface change and decay of sandstone samples exposed to a polluted urban atmosphere over a six-year period: Belfast, Northern Ireland*, **Building and Environment, 38**(9-10), 2003, pp. 1205-1216. DOI: 10.1016/s0360-1323(03)00077-5.
[20] Z.B. Ke, X.G. Yang, L. Ye, Y. Huang, H.P. Xing, PJ. Jin, *Research on Weathering and Influence of Prior Protective Coating above the Outdoor Stone Sculpture in Chongqing*, **Spectroscopy and Spectral Analysis, 37**(10), 2017, pp. 3229-3234. DOI：10．3964／j．issn．1000-0593(2017)10-3229-06.
[21] A.B. Gaikwad, C.B. Rajput, *Effect of Carbonation on High Strength Concrete*, **International Journal of Engineering Research and Technology, 6**(6), 2017, pp. 159-162. DOI: http://dx.doi.org/10.17577/IJERTV6IS060149.
[22] F. Balsamo, F.H.R. Bezerra, M.M. Vieira, F. Storti, *Structural control on the formation of iron-oxide concretions and Liesegang bands in faulted, poorly lithified Cenozoic sandstones of the Paraiba Basin, Brazil*, **Geological Society of America Bulletin, 125**(5-6), 2013, pp. 913-931. DOI: 10.1130/b30686.1.
[23] N. Marinoni, M.P. Birelli, C. Rostagno, A. Pavese, *The effects of atmospheric multipollutants on modern concrete*, **Atmospheric Environment, 37**(33), 2003, pp. 4701-4712. DOI: 10.1016/j.atmosenv.2003.06.001.
[24] J. Madejova, P. Komadel, *Baseline studies of the clay minerals society source clays: infrared method*, **Clays and Clay Miners, 49**, 2001, pp. 410–432. DOI: 10.1346/ccmn.2001.0490508.
[25] S. Chhaiba, M.T. Blanco-Varela, A. Diouri, S. Bougarrani, *Characterization and hydration of cements and pastes obtained from raw mix containing Moroccan oil shale and coal waste as a raw material*, **Construction and Building Materials, 189**, 2018, pp. 539-549. DOI: 10.1016/j.conbuildmat.2018.09.014.
[26] S. Guggenheim, *Baseline Studies of the Clay Minerals Society Source Clays: Thermal Analysis*, **Clays and Clay Minerals, 49**(5), 2001, pp. 433-443. DOI: 10.1346/ccmn.2001.0490509.
[27] PJ Jin, Y. Zhang, S. Wang, X.G. Yang, M. Zhang, *Characterization of the superficial weathering of bricks on the City Wall of Xi'an, China*, **Construction and Building Materials, 149**, 2017, pp. 139-148. DOI: 10.1016/j.conbuildmat.2017.05.045.
[28] M. Escudey, P. Díaz, G. Galindo, A.C. Chang, *Differential thermogravimetric analysis of oxalate in hydrogen peroxide‐treated allophanic soils*, **Communications in Soil Science and Plant Analysis, 30**(7-8), 1999, pp. 937-946. DOI: 10.1080/00103629909370258.
[29] K. Baltakys, T. Dambrauskas, D. Rubinaite, R. Siauciunas, A. Grineviciene, *Formation and hydration of eco-friendly cement using industrial wastes as raw materials*, **Scientific Report, 11**(1), 2021, Article Number: 14742. DOI: 10.1038/s41598-021-94148-x.

[30] K.H. Friolo, A.S. Ray, B.H. Stuart, P.S. Thomas, *Investigation of the degradation of sandstones in Sydney's heritage buildings*, **Structural Analysis of Historical Constructions**, 2005, pp. 239-244.
[31] K.H. Ip, B.H. Stuart, P.S. Thomas, A.S. Ray, *Thermal characterization of the clay binder of heritage Sydney sandstones*, **Journal of Thermal Analysis and Calorimetry, 92**(1), 2008, pp. 97-100. DOI: 10.1007/s10973-007-8743-y.
[32] A.F. Plante, J.M. Fernández, J. Leifeld, *Application of thermal analysis techniques in soil science*, **Geoderma, 153**(1-2). 2009, pp. 1-10. DOI: 10.1016/j.geoderma.2009.08.016.
[33] D. Ruiz-Serrano, M. Flores-Acosta, E. Conde-Barajas, D. Ramírez-Rosales, J.M. Yáñez-Limón, R. Ramírez-Bon, *Study by XPS of different conditioning processes to improve the cation exchange in clinoptilolite*, **Journal of Molecular Structure, 980**(1-3), 2010, pp. 149-155. DOI: 10.1016/j.molstruc.2010.07.007.
[34] M. Nuño, G.L. Pesce, C.R. Bowen, P. Xenophontos, R.J. Ball, *Environmental performance of nano-structured $Ca(OH)_2/TiO_2$ photocatalytic coatings for buildings*, **Building and Environment, 36**, 2015, pp. 734–742. DOI: 10.1016/j.buildenv.2015.05.028.
[35] Konno H, Sasaki K, Tsunekawa M, Takamori T, Furuichi R, *X-Ray photoelectron spectroscopic analysis of surface products on pyrite formed by baterial leaching*, **Bunseki Kagaku, 40**(11), 1991, pp. 609-616. DOI: 10.1016/0169-4332(91)90088-2.
[36] Y. Natsuki, M. Yoshio, N. Masaru, S. Etsuo, *Salt weathering in residential concrete foundations exposed to sulfate-bearing ground*, **Journal of Advanced Concrete Technology, 8**(2), 2010, pp. 121-134. DOI: 10.3151/jact.8.121.

---

*Received: August 08, 2022*
*Accepted: May 24, 2023*